Percolation versus cluster models for multimode vibration spectra of mixed crystals: GaAsP as a case study

O. Pagès,* J. Souhabi, A. V. Postnikov, and A. Chafi
Laboratoire de Physique des Milieux Denses, Université Paul Verlaine—Metz, 1 Bd. Arago, 57078 Metz, France
(Received 19 December 2008; revised manuscript received 16 June 2009; published 16 July 2009)

We reexamine the phonon mode behavior of GaAsP, the leading system among those alloys that exhibit "anomalous" vibration spectra of the one-bond→multimode type, the sign of a far-from-random substitution if we refer to the 1-bond→4-mode cluster model (microscopic insight), which has been accepted through use. In fact, we show that the phonon behavior of GaAsP obeys a basic version of the 1-bond→2-mode percolation model (mesoscopic insight), just as the phonon behaviors of InGaAs, InGaP, and ZnTeSe [O. Pagès *et al.*, Phys. Rev. B **77**, 125208 (2008)], the leading systems representing the three admitted variants of the "nominal" 1-bond→1-mode type for random alloys as covered by the modified random element isodisplacement model (macroscopic insight). With this, GaAsP and its like are rehabilitated as random alloys in principle, and further, the percolation paradigm generalizes to all types and subtypes of the traditional classification of phonon mode behavior of semiconductor alloys, based on the virtual crystal approximation. The discussion is supported by phenomenological modeling of representative Raman and infrared-reflectivity spectra of GaAsP taken from the literature via the percolation model, *ab initio* insight into the phonon mode behavior of basic impurity motifs, and existing experimental/*ab initio* bond length data.

DOI: 10.1103/PhysRevB.80.035204 PACS number(s): 78.30.Fs, 63.10.+a, 63.20.Pw

I. INTRODUCTION

Since the emergence of $AB_{1-x}C_x$ semiconductor alloys with zincblende structure (A being either an anion or a cation), which takes us more than a midcentury back, Raman and infrared (IR) spectroscopies have been widely used as versatile techniques at the laboratory scale to access the vibrational properties. The field is well-documented: the corpus of data is large, and several models were developed for their basic understanding.[1–3] In spite of such effort the lattice dynamics of alloys is usually taken as intrinsically complicated. Before presenting the simplest and thus most consensual classification of phonon behavior, where no less than four types are yet distinguished, and being critical about it, we find it useful to indicate from which special angle we reexamine the Raman and IR data in the literature. The basic models used for their discussion will then be outlined from the same angle, for sake of consistency.

First, the experimental aspect. Raman and IR spectroscopies operate at the center of the Brillouin zone ($q \sim 0$), where only optical modes have a propagating character. These consist of counterphase vibrations of the quasirigid A and (B, C) sublattices (with different amplitudes for the B and C species), being either perpendicular [transverse optical (TO) mode] or parallel [longitudinal optical (LO) mode] to the direction of propagation. TO modes consist of purely mechanical vibrations, thus fully decoupled in the harmonic approximation. As such, they carry safe information on individual oscillators present in the crystal. The TO frequency, which scales as the square root of the bond force constant, reveals the nature of each oscillator; the TO intensity gives the population. The LO modes are a complicated issue, at least in multioscillator systems such as alloys, as they carry a Coulombian field $\vec{E}$ due to the ionicity of the bond. When the LO modes are close they do $\vec{E}$ couple, which dramatically distorts the underlying LO signal. Certain LO modes may even virtually vanish, resulting in an oversimplified interpretation.[4] In this work we reaffirm a basic position to focus on TO modes when addressing the key issue of the nature of the phonon behavior of an alloy; the discussion of LO modes follows straightforwardly.[4]

A specific TO insight can be achieved by Raman analysis depending on the scattering geometry. Proper selection rules are given, e.g., in Ref. 5. What is measured by IR absorption is the oscillator strength, a dimensionless parameter that basically relates to the TO-LO splitting of an oscillator. In usual IR reflectivity spectra taken at quasinormal incidence on bulk crystals, such as those discussed in this work, the TO frequency corresponds to the onset of maximum reflectivity; a more accurate insight can be gained from a proper fit of the spectrum to an oscillator model.

Now, the theoretical aspect. The restriction to $q \sim 0$ makes the modeling of a lattice vibration simple. First, the space-related phase of a plane wave describing an ideal phonon vanishes at $q \sim 0$, and with it an obligation to position an atom in the crystal with vectors. Therefore, in writing the equations of motion per atom, a model based on a scalar representation of the crystal (linear chain approximation), a phenomenological one then, should do in principle. In this case the relevant oscillators regarding out-of-phase motions of the A and (B, C) rigid sublattices are the A-B and A-C bonds, and it all comes down to a question of bond stretching force constants. Second, at $q \sim 0$ the LO-like field $\vec{E}$ is spatially averaged over one unit cell. Its propagation can thus be simply formalized via Maxwell equations, which bear upon quantities having meaning at a macroscopic scale only. The models discussed in this work were all built up on the above basis, and thus can be directly compared one with another.

In principle, several oscillators may exist per bond. Indeed, while it is well known that a bond tends to keep its natural length in an alloy,[6] some adaptation is nevertheless required to accommodate the local mismatch in A-B and A-C

bond lengths. Different neighborhoods may induce different bond lengths, leading to as many $q \sim 0$ TO modes. This is because, within a given bond species, the bond force constant varies with bond stretching (elastic interactions are not really harmonic). A simple rule is that *short bonds have a large force constant and thus vibrate at high TO frequency*, and vice versa. According to the Anderson's criterion, such so-called phonon localization (i.e., multi $q \sim 0$ TO modes per bond) occurs only if the fluctuation in the TO frequency is larger than the TO dispersion,[7] the dispersion in the pure crystal constituting a natural reference.

In time with the massive emergence of zincblende alloys, two phenomenological models were proposed, i.e., the 1-bond→1-TO "modified random element isodisplacement" (MREI) model from Chang and Mitra,[8] and the 1-bond→4-TO cluster model from Verleur and Barker (VB).[9,10] These have persisted so far, and support the basic classification of phonon behavior of semiconductor alloys into four main types (see below). The essentials of each model are summarized hereafter, in order to set up a common jargon for the discussion, and also to put the subsequent introduction of our alternative model, i.e., the so-called 1-bond→2-TO percolation model,[4] into a proper perspective.

MREI model. Most $AB_{1-x}C_x$ alloys were found to obey the MREI model. In this model, bonds of like species (A-B or A-C) are taken as equivalent at a given x value, which comes to assume that the Anderson's criterion is never fulfilled. We thus refer to the MREI model as a *macroscopic* model. In practical terms, the MREI model works as if all individual A-B and A-C bonds were immersed into the same continuum whose properties are locally averaged depending on x, according to the virtual crystal approximation (VCA). This generates distinct A-B and A-C TO modes, each one shifting smoothly between the limits of being either an impurity mode (ω_{imp}) or the zone-center bulk TO mode when x varies; the intensities scaling as the corresponding bond fractions. The zone-center bulk TO frequencies being generally well known, only one input parameter is thus needed per bond to formalize the above trend, namely, ω_{imp}. The short (long) bond is tensed (compressed) when immersed into a crystal with a large (small) lattice constant, which decreases (increases) the TO frequency. In a TO frequency versus x plot the A-B and A-C TO branches should thus be quasiparallel. As an effect of the VCA, no singularity is expected in the phonon behavior with respect to neither the frequency nor the intensity. Such 1-bond→1-TO MREI-VCA type[11] is outlined in Fig. 1 (refer to thick lines and to ovals). A more complete scheme is given in Ref. 4 (Figs. 1 and 2 therein).

When confronted with experiment, the 1-bond→1-TO MREI-VCA type divides into three subtypes, specifying for each type the leading system in brackets:[12] (i) pure 1-bond →1-TO (InGaAs), (ii) 2-bond→1-TO (ZnTeSe) and, exceptionally, (iii) modified-2-TO (InGaP, Ref. 13). Synthetic schemes are given, e.g., in Fig. 2 of Ref. 4. A criterion based on the coherent potential approximation (CPA) was worked out by Elliott *et al.*[2] to distinguish between the two main types. Type (i) appears when the A-B and A-C TO-LO bands built up by linear interpolation of the parent TO and LO frequencies onto the impurity one (shaded areas in Fig. 1) do not overlap, type (ii) otherwise. Globally, the MREI-VCA (experimental) and Elliott-CPA (theoretical) classifications were found to be consistent (see a detailed review in Ref. 1).

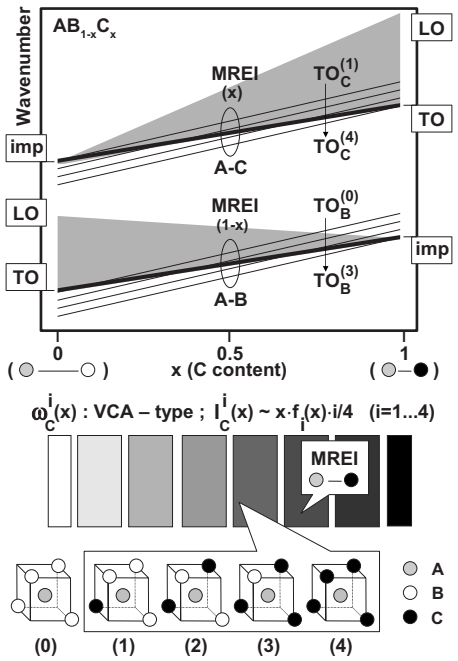

FIG. 1. Cluster type description of a random $AB_{1-x}C_x$ crystal in terms of five possible A-centered cluster units labelled i=0–to–4 according to the number of C atoms at the corners (lower panel). The VCA-type host medium is schematically represented by a gray-scale. The corresponding 1-bond→4-TO mode behavior is shown in the upper panel. The generic forms of the TO-(frequency ω, intensity I) x dependencies for each relevant cluster type (superscript i) are summarized above the crystal drawing by putting an emphasis on the short A-C bond (subscript C). The native bond lengths are schematically indicated at $x \sim 0,1$. For a given bond the TO frequencies (thin lines) are ranked from top to bottom in the sense of the increasing fraction of the short bond in the clusters. The intensity of an individual TO mode scales as the total fraction of like bonds, i.e., as x for A-C and $(1-x)$ for A-B, weighted by both the fraction $f_i(x)$ of the host cluster in the crystal and the fraction of like bonds in that cluster, i.e., $i/4$ for A-C and $(4-i)/4$ for A-B. The corresponding MREI dependencies (ω: thick lines, I: within brackets) are also shown (upper panel), for comparison. For sake of completeness the TO-LO bands used for the Elliott's criterion are indicated (shaded areas). Counterparts of the lower and upper panels for the percolation model are shown in Figs. 1(b) and 5(a) of Ref. 4.

A different class was nevertheless required, of main interest in this work, for those rare alloys that do exhibit obviously more than one TO mode per bond in their vibration spectra, thereby falling out of the MREI scope. The most representative zincblende alloy is $GaAs_{1-x}P_x$. The two pioneer series of IR reflectivity spectra taken with this alloy by VB (Ref. 9) and by Chen, Shockley, and Pearson (CSP) (Ref. 14) show two well-resolved resonances for the short Ga-P bond, spaced by $\sim 20\ \mathrm{cm}^{-1}$. The same applies to the short Cd-S bond in $CdS_{1-x}Se_x$ that crystallizes in the wurtzite structure.[10]

Cluster model. To model such "special" behavior in $AB_{1-x}C_x$ zincblende crystals, VB came to discriminate be

tween the force constants of like bonds depending on the A-centered $AB_{4-i}C_i$ tetrahedral cluster they belong to, $i=0,\ldots,4$. The idea is that differences in A first neighbors are sufficient to create phonon localization. We thus refer to the cluster model as a *microscopic* model.

In writing the equations of motion, VB consider isodisplacement of like atoms in like clusters, and push the force assessment to the nearest-neighbor cluster. The VCA is explicit at two levels in these equations: at the cluster level, as the nearest-neighbor cluster is averaged over all possible ones depending on the fraction $f_i(x)$ of cluster i at alloy composition x (an explicit form is given in Ref. 9), and also at the atom level, as a substituting atom in each cluster, i.e., the considered one plus the nearest-neighbor one, virtually represents B and C in proportion to their fractions in that cluster [$i/4$ for C and $(4-i)/4$ for B]. Basically, instead of two series of equivalent bonds (A-B and A-C) immersed in a VCA-type continuum, as in the MREI model, this comes to imagine five series of equivalent clusters (i-numbered) embedded in that continuum (see Fig. 1). This ends up with five $f_i(x)$-dependent equations per invariant (A) atom, and with four equations per B and per C atom, i.e., one per cluster hosting such atoms. Out of these, eight A-B and A-C bond-stretching equations, referring to out-of-phase motions of A against B and C, thus Raman and IR active modes, can be derived.[15] On top of the [(i)–(iii)] MREI subtypes, this leads to a (iv) 1-bond→4-TO cluster type.[16]

Hence, the cluster model splits each MREI-like TO branch into four sub-branches. These are quasiparallel in force of the same argument used for the MREI model. A basic rule supported by *ab initio* calculations[17] is that bonds are longer (shorter) in environments rich of the shorter (longer) bond. Accordingly, in a TO frequency versus x plot the four TO branches per bond should rank from top to bottom in the sense of the increasing fraction of short bonds in the clusters. Note that such ideal order is not strictly respected for the Ga-P bond in the GaAsP cluster scheme (see Fig. 6 of Ref. 9), while it is for the Cd-S one of CdSSe (see Fig. 16 of Ref. 10). The strength of a TO mode, as for it, scales as the fraction of related bond, i.e., as x for A-C and as $(1-x)$ for A-B, weighted by both the fraction of the host cluster $f_i(x)$ and the fraction of the considered bond in that host cluster [$i/4$ for C and $(4-i)/4$ for B]. Following from the VCA, no singularity is expected in the TO-frequency/intensity dependencies on x. The content of the cluster-VCA model is summarized in the bottom of Fig. 1, with the related TO mode behavior outlined in the top panel.

In principle, four TO modes per bond should be more than enough to explain what seems to be a mere bimodal fine structure in the IR response of the short Ga-P bond of $GaAs_{1-x}P_x$. In fact, fair modeling of the IR reflectivity spectra of this alloy via the cluster model, "*still by no means exact*" quoting VB (Ref. 9, p. 727), could be achieved only by assuming an over-representation of the As-rich and P-rich clusters to the detriment of the (As, P)-mixed ones, at any x value.[9] A similar condition applies to $CdS_{1-x}Se_x$.[10] The deviation with respect to the nominal balance in case of random As↔P (S↔Se) substitution was estimated by introducing a short scale order parameter β varying between 0 (random crystal) and 1 (phase-separated crystal), which increases the probability of finding a substituting atom next to a substituting atom of the like species. Explicit $f_i(x,\beta)$ laws were derived by VB.[9] β was found to be large for GaAsP (0.75) (Ref. 9) and CdSSe (0.40),[10] suggesting large local clustering.

Since then, on the basis of the cluster-VCA model, a 1-bond→multi-TO behavior in the vibration spectra of an alloy was taken as "anomalous," the sign of a far-from-random substitution. As opposed to this, the basic 1-bond →1-TO type, as covered by the MREI-VCA/Elliott-CPA scheme, has emerged as the "nominal" type for random alloys.

However, there are problems with such MREI/cluster-VCA classification. Our reexamination of the Raman and IR data in the literature has revealed that even the leading alloys of the generic MREI-VCA type do not show the three variants, (i) to (iii), that they are supposed to represent.[4] The problem with GaAsP and its like, of the cluster-VCA type (iv), is different, namely, they look random in every other respect than their vibrational properties. No significant clustering could ever be detected in GaAsP by other techniques, such as x-ray microprobe analysis, Auger spectroscopy or extended x-ray absorption fine structure (EXAFS) measurements.[18] VB themselves admit that their samples "*show no large scale clustering*" (Ref. 9, p. 716). Further, CSP indicate after careful x-ray diffraction and band-edge absorption analysis that samples grown by vapor phase epitaxy, such as theirs and those from VB, are "*free of gross inhomogeneities in the distribution of the constituent atoms*" and "*excellent for the study of phonon spectra in disordered systems*" (Ref. 14, p. 649), i.e., in random ones. This has lead Robouch *et al.* to challenge seriously the cluster-VCA model recently.[18] More fundamentally, Elliott *et al.* stated that the cluster-VCA model is "*not physically realistic*" (Ref. 2, p. 526), though without explaining the reason behind their statement. Probably, this relates to the attribution by VB of one TO mode per bond and per cluster whatever the bond configuration inside the cluster. Indeed, in such a cluster-embedded-into-continuum approach as the cluster-VCA, where the cluster is taken as the elementary vibrating unit (instead of the bond unit as in the MREI-VCA scheme), one is facing a sort of molecular-type problem in principle, and the phonon picture might be more complicated. In fact, our recent *ab initio* calculations show that already a pair of connected impurity bonds in a pure crystal gives three distinct vibration modes at $q\sim 0$, not only one. These consist of atom vibrations longitudinal and transverse (in-plane and out-of-plane) to the chain (see, e.g., Fig. 1 in Ref. 19), the latter two being quasidegenerate in general (see Fig. 6 in Ref. 4). This is enough *per se* to establish that the cluster-VCA model is not conceptually valid.[20]

By definition, phonons reveal the lattice dynamics, i.e., collective vibration modes, so that one cannot escape a sort of average description of the alloy disorder at a certain stage. In the MREI and cluster schemes this is apparent in the VCA-type representation of the crystal. Now, ultimately phonons refer to the bond force constant, which is a local physical property. As such, a proper understanding should also incorporate some insight into the topologies of the substituting atoms. The crucial problem, then, is how to concili-

ate into a unique picture this apparent duality of phonons as a collective (lattice vibration)/local (bond-related) physical property. In the MREI approach (macroscopic insight) the local character of the bond force constant is denied; only the collective aspect is taken into account, i.e., via the VCA-like uniformity of the lattice. In contrast, the cluster model (microscopic insight) comes to a molecular-type approach, and as such takes into account some local aspect. However, put to the ultimate test of *ab initio* calculations, it just appears to be not physically realistic (see above), as anticipated by Elliott *et al.* (Ref. 2, see above).

Percolation model. As an intermediate approach, one of us (O.P.) has developed in recent years a so-called percolation model. This can be viewed as a sort of sophistication to the mesoscopic scale of the original MREI-VCA model that operates at the macroscopic scale. In this model a (macroscopic) $AB_{1-x}C_x$ alloy is described as a composite of the B-like and C-like sub (mesoscopic) alloys where *A*-B and *A*-C bonds are more self-connected, respectively, as a result of natural fluctuations in the x value at the local scale. Different bond lengths in the two regions, i.e., of the order of 1% per bond from *ab initio* calculations,[21] seem sufficient to create phonon localization. This introduces a 1-bond$\rightarrow$2-TO type. The local and collective aspects of phonons are conciliated in such *mesoscopic* model, in that the dependence on different environments (B- and C-like regions) is explicit (local aspect), and the environments in question are defined via an explicit concept of connectivity (collective aspect). Some VCA-type averaging of each region is also there, albeit on restricted x domains (continuum regime, see below). One may imagine two interlaced treelike networks (the B- and C-like regions) that are coupled via the lattice, but with slightly different eigenfrequencies of vibration.

In a TO frequency versus x plot each MREI TO branch splits into a symmetrical double branch. The lower subbranch refers to the region "possessing" the short bond (same argument as for the cluster model), and in total the four sub-branches go with x quasiparallel (same argument as for the MREI model). Each C-like (B-like) sub-branch exhibits a singularity at $x_C=0.19$ ($x_B=0.81$), the *A*-C (*A*-B) bond percolation threshold (PT).[22] This is due to a change in the internal structure of the C-like region from quasistable ($x<$PT, fractal-like regime) to smoothly x dependent ($x>$PT, normal regime) when this region turns from a dispersion to a continuum.[23] In fact the continuum is described as a suballoy by using a standard MREI-VCA approach, but rescaled to the composition domain of the normal regime. The TO intensity scales as the related *A*-C (x) or *A*-B ($1-x$) bond fraction, weighted by the scattering volume of the host C- (x) or B-like ($1-x$) region. Two input parameters per bond fix the whole trend, i.e., ω_{imp}, as for the MREI model, plus the splitting Δ between the like TO modes from the B- and C-like regions in the dilute limits. Usually Δ is finite for the short bond and negligible for the long one. This is because short bonds generally involve small atoms that may adapt their position to accommodate the local difference in *A*-B and *A*-C bond lengths. Such bonds may thus suffer a large distortion when changing from the B- to the C-like region, with concomitant impact on Δ. The essentials of the percolation model are outlined in Fig. 1(b) of Ref. 4, the corresponding TO behavior being depicted in Fig. 5(a) therein.

Recently, we have shown that the apparent anomalies in the vibration spectra of the *random* InGaAs, ZnTeSe, and InGaP, (i) to (iii), MREI alloys can be explained within the percolation model.[4] In this work we investigate whether this model may also account for the multiphonon spectra of GaAsP based on *random* As$\leftrightarrow$P substitution. Our ambition is twofold. First, it is a matter to extend our percolation model to the leading alloy of the remaining (iv) cluster type, which would complete a unification of the phonon behavior of semiconductor alloys within the percolation paradigm. Second, by passing, we aim at rehabilitating GaAsP and its like as random alloys regarding their vibrational properties.

The manuscript is organized as follows. In Sec. II we derive a version of the percolation model for $GaAs_{1-x}P_x$ that fits the observed x dependencies of the TO and LO frequencies. In Sec. III we perform *ab initio* bond length and phonon calculations to secure our experimental ($\omega_{\mathrm{imp}}, \Delta$) estimates as inferred from the "TO frequency versus x" percolation map (Sec. II). In Sec. IV we compare theoretical vibration spectra calculated via the percolation model with representative data taken from the literature. Reference percolation-based TO and LO Raman line shapes are first produced, as a basis for the discussion (Sec. IV A). LO-pure Raman data are then reexamined, with special attention to the unassigned mode *X* in the literature (Sec. IV B). Then, we turn to the original IR reflectivity spectra from VB (Sec. IV C), i.e., the very ones that did motivate the development of the cluster-VCA model. In Sec. V we conclude by a critical evaluation of the "MREI-VCA/Elliott-CPA+cluster-VCA" classification in the light of the percolation model.

II. PERCOLATION SCHEME FOR RANDOM $GaAs_{1-x}P_x$

The lattice mismatch $\Delta a/a$ in GaAsP ($\sim 3\%$) is less than in InGa(As,P) and in ZnSeTe ($\sim 7\%$), which seems less favorable to phonon localization. However, the TO mode has no dispersion in GaP, shifting by only ~ 1.5 cm^{-1} from the zone center to the (X) zone edge. Thus, even small variations in bond length may create Ga-P phonon localization, leading to a finite Δ value. This might not be true for Ga-As as, first, it is the long bond (refer to Sec. I), and second the dispersion in the pure crystal is large (~ 15 cm^{-1}). Natural references are Δ_{As} and Δ_{P} in InGaAs and in InGaP, respectively, the subscript referring to the bond. Since $\Delta_{\mathrm{As}} \sim 0$ cm^{-1} in InGaAs (Ref. 4) where Ga-As is the short bond and $\Delta a/a$ is large, we expect *a fortiori* $\Delta_{\mathrm{As}} \sim 0$ cm^{-1} in GaAsP, where this time Ga-As is the long bond and $\Delta a/a$ is small. Now we turn to Ga-P, the short bond in InGa(As,P). As $\Delta a/a$ is small in GaAsP, the difference in Ga-P bond length from the B- to the C-like region is expected to be less dramatic than in InGaP, hence, a smaller Δ_{P} value in GaAsP than in InGaP ($\Delta_{\mathrm{P}} \sim 22$ cm^{-1}, Ref. 4). In summary we anticipate a three-oscillator version of the percolation model for GaAsP, with one MREI-like Ga-As oscillator ($\Delta_{\mathrm{As}} \sim 0$ cm^{-1}) at low frequency (long bond) plus a distinct Ga-P percolation doublet ($0 < \Delta_{\mathrm{P}} \leqslant 22$ cm^{-1}) at high frequency (short bond). This is consistent with the IR data of VB (Ref. 9) and CSP (Ref. 14) (see Sec. I).

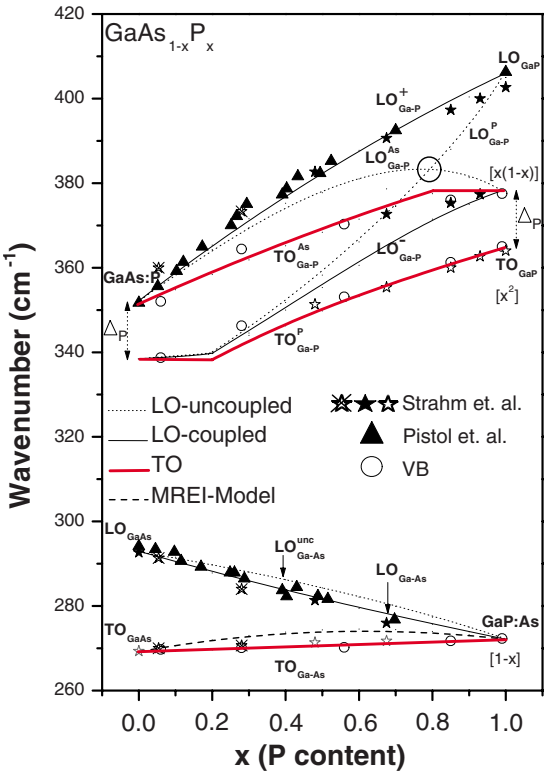

FIG. 2. (Color online) TO (thick-red lines)/LO (coupled–thin lines, uncoupled–dotted lines) percolation scheme of $GaAs_{1-x}P_x$ as built up from representative frequency sets related to pure-TO (open symbols), pure-LO (filled symbols), as well as undetermined-symmetry (crossed symbols) modes in the literature [circles: VB–Ref. 9, stars: Strahm and McWorter–Ref. 24, triangles: Pistol and Liu–Ref. 25]. The data from Ref. 25 were uniformly blueshifted by 2.7 cm^{-1} so that the TO frequency in the pure GaP crystal, chosen as an arbitrary reference, matches 365 cm^{-1} for all three data sets. In the Ga-As spectral range the TO frequency vs x dependency is better described by a straight line (thick line) than by the proper MREI curve (dashed line). The alloy-related LO-(uncoupled—"unc," coupled) curves were subsequently calculated on this simplified TO basis. The fraction of oscillator per TO branch, which fixes the intensity of each individual TO mode, is indicated within square brackets. The circle marks a strong $\vec{E}$-coupling regime in the Ga-P spectral range. In the labeling of the modes, the (Ga-As, Ga-P) subscripts and (As,P) superscripts refer to the bond species and to the host region, respectively. Superscripts "−" and "+" refer to coupled modes.

Representative sets of TO (open symbols) and LO (filled symbols) frequencies of GaAsP are shown in Fig. 2. TO modes as allowed Raman features are rare in the literature. We are only aware of the pioneer data from Strahm and McWorter,[24] as recorded with some of the bulk crystals used by CSP (Ref. 14) in their IR work. Among the (TO,LO) frequency sets displayed in Fig. 5 therein, we select those data that, after reexamination of the literature, do seem intrinsic, i.e., not sample dependent (stars in Fig. 2). Additional TO frequencies were taken from the [1 × (Ga-As), 2 × (Ga-P)] dominant resonances revealed by VB (circles) after curve fitting of their IR data via their own cluster model (see Figs. 9–13 of Ref. 9). A similar TO frequency set was quoted by CSP (Ref. 14) in their Table I. While this is remarkably consistent with the VB set, the CSP data are not shown in Fig. 2 because we find it not pertinent to treat on equal footing raw IR-reflectivity data (CSP ones) and IR-reflectivity data extracted from curve fitting (VB ones). Regarding LO modes, we further consider the data set collected by Pistol and Liu[25] from their pure-LO Raman spectra taken with GaAsP samples of the next generation, i.e., fully relaxed layers grown by metal organic vapor phase epitaxy. The TO frequency of the pure GaP crystal was chosen as an arbitrary reference for all three data sets, and adjusted so as to match the value used by VB (∼365 cm^{-1}). In particular this required to translate upwards by 2.7 cm^{-1} the original set of (Ga-As, Ga-P) LO frequencies from Ref. 25, the resulting TO-LO splitting of pure GaP corresponding then to 365–405 cm^{-1}.

The $(\omega_{\text{imp}}, \Delta)$ input parameters of the percolation model were then derived as follows for each bond. The GaAs:P ($x \sim 0$) and GaP:As ($x \sim 1$) impurity frequencies were identified by convergence of the like TO and LO branches in the dilute limits. The abundant data in Fig. 2 lead to the values of ∼351 cm^{-1} and 272 cm^{-1}, respectively.

Independent insight is derived from the impurity bond lengths via the following equation:

$$\frac{\Delta\omega_T^2}{\omega_T^2} = -6\gamma_T\frac{\Delta l}{l}, \tag{1}$$

which links the difference between the square frequencies of a parent TO mode and of the like impurity mode ($\Delta\omega_T^2$) to the corresponding difference in bond length (Δl), via the TO mode Grüneisen parameter in the pure crystal (γ_T). Experimental insight into Δl is given by existing EXAFS data covering the whole composition range of GaAsP.[26] These indicate that each bond length remains basically stable in the alloy, as usual. Only, the short Ga-P (long Ga-As) bond is slightly tensed (compressed) with increasing As (P) content, due to lattice expansion (shrinking). The impurity bond lengths are inferred from linear interpolation from the parent to the dilute limits. The Δl and corresponding ω_{imp} values are shown in Table I. The γ_T values of GaAs (1.39) and GaP (1.09) were taken from Ref. 27. The agreement is good with the Raman/IR ω_{imp} estimates, the difference is less than 9 cm^{-1}.

Now we turn to Δ. A unique MREI-like Ga-As TO branch joins the parent (TO) and impurity modes, which comes to $\Delta_{\text{As}} \sim 0$ cm^{-1}. In contrast, two distinct Ga-P TO branches appear symmetrically on each side of the virtual line that joins the parent and impurity modes, indicating a finite Δ_{P} value. This is estimated at ∼12 cm^{-1} from the observed Ga-P splitting at both the As- and P-dilute limits. Independent *ab initio* insight into $\Delta_{\text{As,P}}$ is given in Sec. III.

The TO frequency versus x curves derived via the percolation model from the above $(\omega_{\text{imp}}, \Delta)$ values are superimposed to the data in Fig. 2 (thick-red lines). Globally the agreement is good. Note that the Ga-P double branch is quasisymmetrical, as ideally expected (refer to Sec. I). In the Ga-As spectral range we must admit that the agreement is not as good since the actual MREI-like TO curve (dashed

TABLE I. Input parameters of the percolation model for $GaAs_{1-x}P_x$, obtained experimentally [$(\omega_{\text{imp}},\Delta)$, from the raw Raman/IR data], via Eq. (1) [ω_{imp}, by using Δl values either measured by EXAFS (Ref. 26) or calculated by *ab initio* (Ref. 33)] and from direct *ab initio* calculations of the ZC TO-DOS [$(\omega_{\text{imp}},\Delta)$, following a home-made *ab initio* protocol]. Subscripts As and P used for Δl (the difference between the parent and impurity bond lengths, the parent value being quoted first) and Δ (the splitting between like TO modes in the dilute limits) refer to the bond species. Explicit notations of the frequencies of the impurity modes (ω_{imp}) are GaAs:P ($x\sim 0$) and GaP:As ($x\sim 1$).

	$GaAs_{1-x}P_x$				
	EXAFS	*Ab initio*			Raman/IR
Δl_{As} (Å)	2.446–2.428[a]	2.447–2.420[b]	2.456–2.436		
Δl_{P} (Å)	2.359–2.372[a]	2.360–2.382[b]	2.349–2.367		
GaP:As (cm^{-1})	~277[c]	~281[c]	~278[c]	~269	~272
GaAs:P (cm^{-1})	~360[c]	~356[c]	~358[c]	~364	~351
Δ_{As} (cm^{-1})				~0	~0
Δ_{P} (cm^{-1})				~10	~12

[a]Reference 26.
[b]Reference 33.
[c]Derived from Eq. (1).

line) slightly overestimates the data. Now, the deviation does not exceed 3.5 cm^{-1} ($x\sim 0.5$), which is reasonable in view of the simplicity of our model. Nevertheless, as we need a firm TO basis for subsequent discussion of the LO modes in Sec. IV, we prefer to implement the percolation model in the Ga-As spectral range by approximating the TO branch to a straight line that fits perfectly the data (thick line). The GaAs-like LO branch derived on this simplified TO basis then also fits perfectly the data (thin line).

To complete the TO-frequency picture in Fig. 2, we add the TO-intensity aspect by specifying within brackets the bond fraction per TO oscillator in case of random As↔P substitution. In Fig. 2 the (Ga-As, Ga-P) subscripts and (As, P) superscripts of the TO and LO modes refer to the bond species and to the host (As-like, P-like) region, respectively.

III. *AB INITIO* INSIGHT AT THE DILUTE LIMITS

Our motivation for *ab initio* calculations is to secure our Raman/IR $(\omega_{\text{imp}},\Delta)$ estimates. For unambiguous insight into the bond length and phonon properties of an arbitrary atom motif in relation to the above issue, we place the analysis at the dilute limits. The impurity motif under consideration is then immersed into a host matrix of the other type. Generally 64-atom cubic $2\times 2\times 2$-supercells are well converged in size for an *ab initio* insight into the phonon modes of impurity motives no more complicated than a VB cluster.[28] In such supercell an atom half-way between two translated impurities along the [100] vector is the fourth-nearest neighbor to any of them, and one of us (A.V.P.) checked it earlier in similar systems that the force constants can be reasonably discarded beyond the second-nearest neighbors.[29] Even when a second impurity is added close to the first one at $(\frac{1}{2},\frac{1}{2},\frac{1}{2})$, it falls short of having any second-nearest neighbor common to that of a translated impurity. The unconstrained lattice relaxation in such supercells, yielding a negligible deviation from cubicity regarding the lattice vectors, has been done with the SIESTA method,[30] using local density approximation (LDA) and norm-conserving Troullier-Martins pseudopotentials.[31] Note that semicore Ga3d and As3d states were included as valence ones in the construction of pseudopotentials. The basis set was of "standard" in SIESTA "double zeta with polarization orbitals" quality. Force constants have been accumulated by small trial displacements of all atoms in the supercell, whereby a sampling over sufficiently fine $(2\times 2\times 2)$ k mesh was found essential. The results of the *ab initio* calculations are ($q=0$, i.e., zone center) projected (meaning q of the underlying sphalerite primitive cell) TO vibrational density of states (ZC TO-DOS) of different atomic species, say D,

$$I_D(\omega,q\sim 0)\approx \sum_v L(\omega-\omega_v)\sum_j \left|\sum_{\alpha\in D} A_j^{\alpha}(\omega_v)\right|^2, \quad (2)$$

artificially smeared out of 192 discrete lines ω_v stemming from the calculation with Lorentzian $L(\omega)$, for better visibility. In Eq. (2) α runs over atoms of a selected species D and j over three Cartesian components of vibration eigenvector $A_j^{\alpha}(\omega)$. We emphasize that such ZC TO-DOS curves compare directly to TO Raman spectra, in principle.

Ab initio insight into $(\omega_{\text{imp}},\Delta)$ is then obtained by using the following simple protocol that operates in the dilute limits.[4] To access ω_{imp}, we use a supercell containing one impurity (1—imp. motif). In $AB_{1-x}C_x$ alloys this is the ultimate configuration that refers to an impurity (say B) vibrating in the environment of the other substituting species (the C-like region, then). The impurity bond length (A-B) is estimated after relaxation of the supercell, and ω_{imp} (the AC:B frequency) follows by applying Eq. (1) to the difference (Δl) with the native bond length in the pure (AB) crystal. The direct *ab initio* estimate, noted ω_{imp}^{calc}, is not useful at this stage, due to a well-known bias of the calculation method (LDA) towards slight but systematic overestimate of the bond force constant, and thereby of the TO frequency.[32]

Our *ab initio* estimates of Δl for Ga-P and Ga-As (1—imp. motif) compare nicely to the existing EXAFS (Ref. 26)

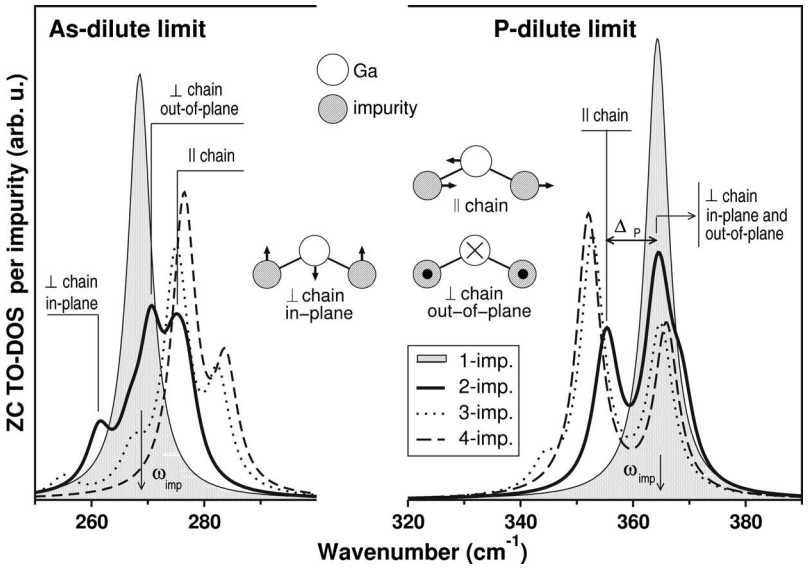

FIG. 3. *Ab initio* ZC TO-DOS per impurity atom of the relevant Ga-centered VB clusters at the *P*-and As-dilute limits. ω_{imp} is indicated in each case. The symbols (∥ chain) and (⊥ chain) refer to out-of-phase cation and anion vibrations along and perpendicular to (in-plane and out-of-plane) the chain of impurity bonds forming the 2—imp. motif (a pair of neighboring substitutional impurities, see text). A finite Δ value is identified for the *P* impurity only (refer to the double arrow).

and *ab initio* (Ref. 33) values, as shown in Table I. The corresponding sets of ω_{imp} values as derived via Eq. (1) are also listed in Table I. The agreement with our Raman/IR estimates (Sec. II) is good. The deviation is less than 9 cm^{-1}.

To access Δ, we use a supercell containing a pair of nearest-neighbor impurities (2—imp. motif). This is the ultimate configuration that refers to an impurity (say B) vibrating in its own environment (the B-like region, then). Generally the triply-degenerate $q\sim 0$ impurity mode (1—imp. motif) splits into two series of pair vibrations (2—imp. motif): a quasidegenerate doublet due to vibrations transverse to the short (B-*A*-B) chain, i.e., in-plane and out-of-plane ones, that usually remains close to the impurity mode, plus a singlet vibration along the chain, that is most separated from the impurity mode. In such ideal case Δ_{B} can be directly estimated from the difference between the *ab initio* frequencies of the singlet (B-*A*-B chain) and impurity (*A*C:B) modes, denoted as $|\omega_{imp}^{pair}-\omega_{imp}^{calc}|$, the LDA blueshift being thus eliminated. A basic rule applies that bonds vibrate at low (high) frequency in environments rich of the short (long) bond, and vice versa (refer to Sec. I), so that $\omega_{imp}^{pair}<\omega_{imp}^{calc}$ ($\omega_{imp}^{pair}>\omega_{imp}^{calc}$) for the short (long) bond.

The ZC TO-DOS curves per impurity of the isolated impurity (1—imp. motif) and of the impurity pair (2—imp. motif) in the P- and As-dilute limits are displayed in Fig. 3. First we focus on the P impurity because the IR spectra of GaAsP exhibit an obvious multimode behavior for the Ga-P bond only (Sec. I). The vibration along the Ga-P chain (2—imp. motif) is well separated from the other P-related modes, i.e., the Ga-P isolated mode (1—imp. motif) plus the doublet mode due to vibrations transverse to the chain (2—imp. motif), the latter three modes being quasidegenerate, as ideally expected. This leads to a well-defined Δ_{P} value of ~ 10 cm^{-1} (see the double arrow in Fig. 3). More confidence into this estimate is obtained by adding to the ZC TO-DOS from the 1—imp. and 2—imp. motifs, which refer to the P-poor VB clusters ($i=1,2$ in Fig. 1), those due to the remaining VB-type motifs with three (3—imp., $i=1,3$ in Fig. 1, dotted line in Fig. 3) and four (4—imp., $i=1,4$ in Fig. 1, dashed line in Fig. 3) P-impurity atoms attached to the same Ga cation. As expected, an addition of the third and fourth P impurities to the same Ga cation leaves the already established two-mode structure (2—imp. motif) basically unchanged. Taken altogether, the ZC TO-DOS per P atom from the 1—to—4—imp. P-motifs leave the overall impression of a robust percolation-type Ga-P TO-doublet with splitting $\Delta_{\mathrm{P}}\sim 12$ cm^{-1}.

Regarding the As impurity, a strict application of the *ab initio* protocol based on the 1—imp. and 2—imp. motifs would lead to a Δ_{As} estimate of ~ 6 cm^{-1}. Yet this can not be considered as a reliable value. Indeed the situation for the As impurity differs from the ideal case in that the pair-related modes (2—imp. motif) split into three equally-spaced features covering a broad spectral range on both sides of the isolated-impurity mode (1—imp. motif). With this the $q\sim 0$ As-modes from the 1—imp. And 2—imp. motifs do not leave the impression of a well-defined percolation doublet. The situation becomes even more complicated by adding the ZC TO-DOS impurity from the 3—imp. and 4—imp. As motifs. The main ZC TO-DOS features then appear to be extremely unstable, being significantly shifted from one impurity motif to another one. This makes it just impossible to define a proper Δ_{As} value. Altogether the As-related ZC TO-DOS should merge into a unique and broad MREI-like feature, corresponding in fact to $\Delta_{\mathrm{As}}\sim 0$ cm^{-1}.

Our *ab initio* estimates of $\Delta_{\mathrm{As,P}}$ are close to the Raman/IR ones (Sec. II), as shown in Table I. The deviation is less than ~ 2 cm^{-1}.

In summary, our *ab initio* insight into $(\omega_{\mathrm{imp}},\Delta)$ secures the frequency aspect of the percolation scheme in Fig. 2.

An interesting question then, if we focus on P, is how does the *ab initio* reality of the P-related phonon behavior at the *atomic* scale connect with the percolation-type description at the *mesoscopic* scale in terms of the As-like and P-like host regions for the P impurities? Rather naturally in fact, if we realize that the isolated P impurity (1—imp. motif) contributes to the high-frequency Ga-P mode only, consistently attributed to the As-like region in the percolation scheme, and, conversely, that the low-frequency Ga-P signal, attributed to the P impurities from the P-like region in the

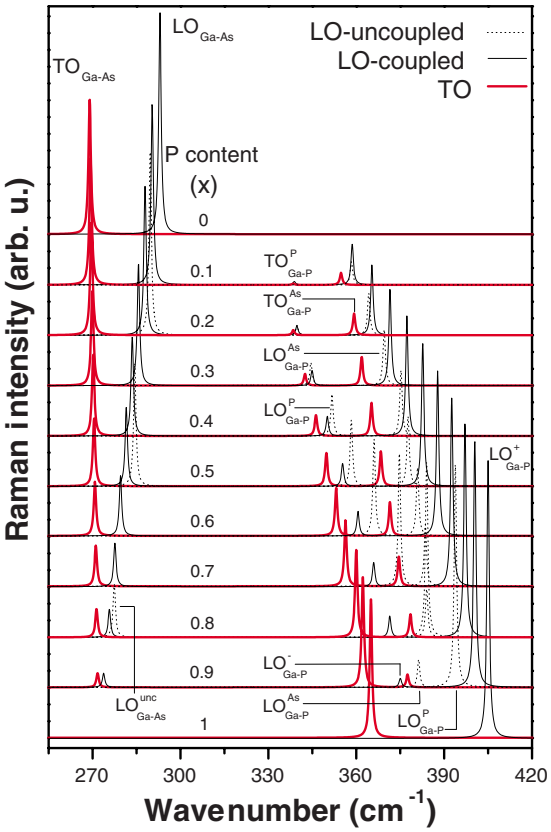

FIG. 4. (Color online) Reference percolation-type TO (thick-red curves), LO-coupled (thin curves), and LO-uncoupled (dotted curves) Raman line shapes of $GaAs_{1-x}P_x$ as derived via Eq. (3) by using the TO-frequency (thick-red curves) and TO-intensity (refer to square brackets) information given per oscillator in Fig. 2. A small (TO, LO) individual phonon damping of ~ 1 cm^{-1} was chosen for a clear overview of the whole collection of oscillators at each x value.

percolation scheme, arises from neighboring P impurities only (2—to—4—imp. motifs).

IV. COMPARISON WITH EXPERIMENT

While the TO-frequency aspect is rather well covered by the percolation scheme in Fig. 2, the TO-intensity aspect, as fixed by the fractions of oscillator in brackets therein, is not validated so far. The ultimate test with this respect is direct confrontation of the model with raw vibration spectra. We naturally refer to those spectra already used to build up the (TO,LO)-frequency map in Fig. 2, i.e., the pure-LO Raman spectra from Pistol and Liu[25] (Sec. IV B), and the pioneer IR reflectivity spectra from VB (Ref. 9) (Sec. IV C). First, as a basis for the discussion, we give some reference insight into the TO and LO Raman line shapes of GaAsP as predicted within the percolation scheme (Sec. IV A).

A. Reference percolation-based (TO,LO) Raman line shapes

For a clear overview of the predicted percolation-type phonon behavior of GaAsP we show in the body of Fig. 4 the theoretical TO (thick lines) and LO (thin lines) Raman line shapes as calculated by injecting the TO-(frequency, intensity) information available per oscillator in Fig. 2 in our usual generic form of the Raman cross section,[4] i.e.,

$$I_{\mathrm{TO,LO}}(\omega,x) \propto \mathrm{Im}\left[-\epsilon_r^{-1}\left(1+\sum_p C_p K_p L_p'\right)^2 + \sum_p C_p^2 \frac{K_p^2 L_p'}{4\pi Z_p^2}\right], \tag{3}$$

that gives TO modes when restricted to its second member, and LO modes when retaining the first member. The summation runs over the three [Ga-As, $(\mathrm{Ga\text{-}P})^{\mathrm{P}}$, $(\mathrm{Ga\text{-}P})^{\mathrm{As}}$] oscillators. The relative dielectric function ϵ_r is accordingly expressed by using a classical series of quasiuniformly damped oscillators. A small damping (~ 1 cm^{-1}) is taken for optimal resolution of the whole collection of oscillators. Still, a slight difference is maintained between the Ga-As and Ga-P dampings, taken in the ratio 5:6 applying to both TO and LO modes, in order to reproduce the intrinsic mismatch in the pure crystals.[34] L'_p, K_p, $4\pi {Z_p}^2$, and C_p, respectively, refer to the classical Lorentzian response of oscillator p, its TO-frequency square, its oscillator strength S_p, as expressed according to the MREI terminology,[8] and its Faust-Henry coefficient. The latter measures the relative scattering efficiencies of the TO and LO Raman p modes.[35] In an alloy, S_p and C_p do scale as the fraction of oscillator p,[4] as specified in brackets in Fig. 2. The starting values in the pure crystals are fixed by the basic observables (TO-LO splitting, ϵ_∞, C), taken as (269–292 cm^{-1}, −0.55, 11.0) and (365–405 cm^{-1}, −0.47, 9.1) for GaAs and GaP, respectively. The TO-LO splitting of GaAs (approximated to the first decimal) and ϵ_∞ values of GaAs and GaP were taken from Ref. 36. Note that the ϵ_∞ value in GaP slightly differs from the original estimate by VB (8.457, Ref. 9). The TO-LO splitting of GaP was estimated in Sec. II. Well-established C values for GaP and GaAs were taken from Refs. 37 and 38, respectively.

The trend for TO modes (Fig. 4, thick curves) is all contained in Fig. 2, regarding both the frequency (thick lines therein) and intensity (terms within brackets therein) aspects. No further discussion is needed.

The situation for the LO modes (Figs. 2–4, thin curves) is not that simple. In the Ga-P spectral range, $\vec{E}$ coupling between the two LO oscillators associated with the TO percolation doublet generates a massive transfer of oscillator strength. This ends up in a "giant" $\mathrm{LO}^{+}_{\mathrm{Ga\text{-}P}}$ mode at high frequency that captures the quasitotality of the available Ga-P oscillator strength, accompanied by a minor $\mathrm{LO}^{-}_{\mathrm{Ga\text{-}P}}$ mode repelled as a residual feature within the native TO double branch. For a clear insight we add to the LO-coupled modes (thin lines) in Figs. 2–4 the original LO-uncoupled ones (dotted lines), the latter being labelled as the related TO modes. The LO cross section of an uncoupled oscillator was calculated via Eq. (3) by restricting ϵ_r to the sole Lorentzian function of that oscillator. A strong $\vec{E}$-coupling regime is identified at $x \sim 0.75$ (marked by a circle in Fig. 2), where quasiresonance conditions for the LO-uncoupled modes give rise to a typical anticrossing of the LO-coupled ones. Some $\vec{E}$ coupling is also present in the Ga-As spectral range, albeit

less dramatic. So, an insight into the LO-uncoupled mode (denoted with superscript "unc" in Figs. 2–4) at the sparse x values of 0.2, 0.5, and 0.8 suffices. There, $\vec{E}$ coupling is evidenced as a slight but systematic redshift of the LO-coupled Ga-As mode with respect to the LO-uncoupled reference. This indicates a non-negligible Ga-As→Ga-P interband transfer of oscillator strength, though the frequency gap between the Ga-As and Ga-P spectral ranges seems forbiddingly large. We checked that no more than ~25% (x=0.8) of the available Ga-As oscillator strength is involved. Note that the agreement between the experimental and theoretical LO frequencies is excellent in Fig. 2, in both the Ga-P and Ga-As spectral ranges.

B. Pure LO Raman spectra: the enigma of the *X* mode

Provided the percolation model applies to GaAsP, we should find, in particular, some systematic track of the $LO^{-}_{Ga\text{-}P}$-$LO^{+}_{Ga\text{-}P}$ doublet in the pure-LO Raman data. A brief review of the literature in this respect reveals the following.

Strahm and McWorter[24] in their pioneer (TO,LO)-mixed Raman spectra observed at moderate-to-low As content a weak but distinct peak, currently referred to as X, within the main TO-LO band, i.e., our $TO^{P,Ga}_{Ga\text{-}P}$-$LO^{+}_{Ga\text{-}P}$ band. From the phonon dispersion of pure GaP (see, e.g., Ref. 39), the best candidate for X was identified as a LO one-phonon density of states at the zone edge (L). Some theoretical support was later provided by Schmetzler and Beserman[40] based on calculations of the localized states in GaAsP at low As content within the Green's function theory.

Hirlimann *et al.*[41] did perform a careful symmetry analysis of X as apparent in their pure-LO Raman spectra at moderate-to-low As content (5–20%). When turning from a LO-allowed to a LO-extinct setup they observed that "*the GaP LO mode* ($LO^{+}_{Ga\text{-}P}$) *and the X band decrease together*" (Ref. 41, p. 209). If X were a zone-edge mode, i.e., a theoretically forbidden feature, it should remain quasi-insensitive to the selection rules at $q\sim0$, which opposes the experimental findings. Hirlimann *et al.* were thus lead to reassign X as an hybrid feature due to anharmonic coupling between the nominal $q\sim0$ discrete LO mode ($LO^{+}_{Ga\text{-}P}$) and some disorder-activated phonon continuum. The similarity in the selection rules of X and of the Ga-P LO mode would then merely reflect the "$q\sim0$ LO side" of the hybrid X mode. However, the discussion remained qualitative only, and neither the phonon continuum nor the coupling mechanism could be identified.

Jain *et al.*,[42] in view of this, stated that the origin of X was uncertain, and recommended further experimental investigation. Since then, we are not aware that the issue of the X mode was ever raised again, though X continued to be detected.[43]

If we focus on experiment, all the ingredients are there to reassign X as $LO^{-}_{Ga\text{-}P}$. X would thus be a nominal $q\sim0$ LO mode, just as $LO^{+}_{Ga\text{-}P}$, which explains the quasisimilarity in their selection rules. Further, as emphasized by all authors, X shows up clearly at moderate-to-small As content only, which is consistent with the $LO^{-}_{Ga\text{-}P}$ mode being relatively strong and well separated from its native $TO^{P}_{Ga\text{-}P}$ branch at this limit only (see Fig. 4). Last, in Fig. 2 the agreement between the data from Strahm and McWorter and the model (compare the filled stars with the thin line at ~370 cm^{-1}) is excellent in the As-dilute limit (~7.5% and ~15% As), and fair at moderate As-content (~32.5% As).

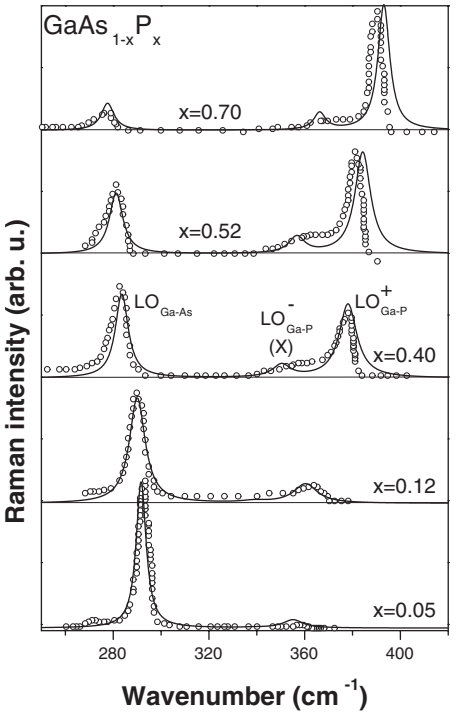

FIG. 5. Comparison of theoretical LO-coupled Raman line shapes for random $GaAs_{1-x}P_x$ (thin lines) calculated by injecting in Eq. (3) the three-oscillator [Ga-As, $(Ga\text{-}P)^{P}$, $(Ga\text{-}P)^{As}$] version of the percolation model displayed in Fig. 2, with corresponding raw LO-pure Raman spectra taken from the literature (symbols, digitized from Fig. 2 of Pistol and Liu–Ref. 25, and uniformly blueshifted by 2.7 cm^{-1} for sake of consistency with Fig. 2).

Now, we consider the next generation of pure-LO Raman spectra, where X is not mentioned. Such spectra were thus routinely discussed within the 1-bond→1-mode MREI scheme. The spectra from Pistol and Liu[25] (Fig. 2 therein) are reproduced in Fig. 5, while being blueshifted by 2.7 cm^{-1} for consistency with the data in Fig. 2 (refer to Sec. II). Careful analysis reveals the X mode as a weak and overdamped shoulder on the low-frequency tail of the $LO^{+}_{Ga\text{-}P}$ mode. The shoulder persists over the whole composition range, but shows up as a distinct feature only for moderate-to-low As contents, as expected (refer to Fig. 4). The shoulder is also present in the pure-LO Raman spectra taken by Armelles *et al.* with partially relaxed $GaAs_{0.77}P_{0.23}$ layers grown by atomic layer molecular beam epitaxy (see Fig. 1 of Ref. 44). The shoulder is thus not merely fortuitous, i.e., due to some specific growth techniques, but actually intrinsic to GaAsP in the LO symmetry.

We superimpose to the data in Fig. 5 the corresponding percolation-type LO Raman line shapes calculated along the same procedure as in Sec. IV A, for comparison. A single adjustable parameter was used per x value, namely, the individual TO damping. This was taken identical for the two Ga-P oscillators because these refer to the same bond, and

close to the Ga-As one because the intrinsic dampings in the pure crystals are similar (see Sec. IV A). A significant departure from the latter constraints occurs only in the moderate-to-dilute limits where the impurity mode(s) may become overdamped, e.g., at $x=0.05$ the Ga-As and Ga-P dampings were found to scale as 5:9. Otherwise the rule is ideally fulfilled, e.g., at $x=0.52$ the dampings scale as 7:8. Some disagreement between the experimental and theoretical Ga-P frequencies in Fig. 4 (refer to $x=0.52$, 0.70), which is absent in Fig. 2, is due in fact to a slight discrepancy in the data source itself [i.e., in Ref. 25, between Figs. 2 and 3(b) therein]. Quasiperfect contour modeling of the Ga-P signal can be achieved just by readjusting slightly the starting TO frequencies within less than ~ 3 cm^{-1} (not shown). In spite of the simplicity of our model, the experimental spectra are rather well reproduced, including the nonquoted X shoulder, which secures an assignment of X as $\mathrm{LO}^{-}_{\mathrm{Ga\text{-}P}}$ on a quantitative basis.

C. Back to the origin of the cluster model: the 1-bond →multimode IR reflectivity spectra of GaAsP

Ultimate insight comes from confrontation of the percolation model with the IR reflectivity spectra of $GaAs_{1-x}P_x$ taken by VB, i.e., the very ones that did motivate the development of the cluster model by the same authors. These spectra provide a (TO,LO)-combined insight, and as such can be used to test the percolation scheme outlined in Fig. 2 as a whole. The IR spectra in Figs. 1 (pure crystals) and 9–12 (mixed crystals) of Ref. 9 were reproduced in Fig. 6 (open symbols). We have superimposed to each spectrum the best adjustment obtained by VB after curve fitting via their cluster model (thin curves). The latter theoretical curves were recomputed by using the standard expression,

$$R(\omega,x) = \left| \frac{1-\sqrt{\epsilon_r}}{1+\sqrt{\epsilon_r}} \right|^2, \tag{4}$$

for the reflection coefficient at normal incidence on a two-layer system (vacuum/GaAsP), and the individual sets of (TO frequency, oscillator strength, TO damping) adjusted per oscillator by VB. The agreement with the data is good, which must not be surprising owing to the large number of adjusted parameters. However, we recall that this could be achieved only by assuming a far-from-random As↔P substitution as reflected by a large β value ($\sim 0,75$). As already mentioned, this does not seem to comply with reality. Besides, an apparent deficiency in the VB treatment is that a basic conservation of the oscillator strength is not exactly fulfilled, as noticed by Robouch *et al.*[18] In principle the available oscillator strength per bond should scale as the related bond fraction,[45] irrespective of the way it distributes among the VB host clusters. As some Ga-As→Ga-P transfer of oscillator strength exists in GaAsP (Sec. IV A), care must be taken that the conservation should be discussed on a per alloy basis rather than on a per bond basis. Still, the oscillator strength per alloy, as inferred from the VB treatment by summing over the Ga-As and Ga-P bonds, does not scale linearly with the alloy composition. This is significantly underestimated (see the negative bowing of the top curves in Fig. 8 of Ref. 9).

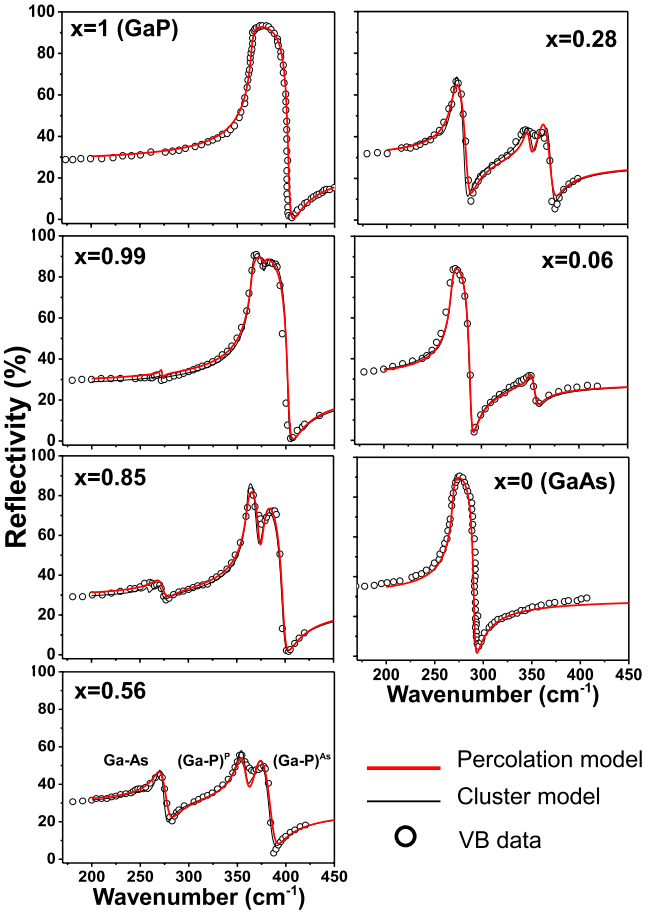

FIG. 6. (Color online) Original series of raw IR reflectivity spectra of $GaAs_{1-x}P_x$ taken by VB (symbols, reproduced from Fig. 1–pure crystals–and Figs. 9 to 13–alloys–of Ref. 9) compared with two series of theoretical curves: cluster model [thin curves, recomputed from Eq. (4) by using the TO-(frequency, oscillator strength, phonon damping) input parameters per oscillator adjusted by VB–see Ref. 9] and percolation model [thick-red curves, calculated by injecting in Eq. (4) the corresponding information as available in Fig. 2, a slight adjustment being allowed for the phonon damping–see text].

In fact, we could achieve a similar agreement with the experimental curves just by injecting in Eq. (4) our three-oscillator [Ga-As, $(\mathrm{Ga\text{-}P})^{\mathrm{P}}$, $(\mathrm{Ga\text{-}P})^{\mathrm{As}}$] percolation-type relative dielectric function, as built up from the TO-(frequency, intensity) information given per oscillator in Fig. 2 (thick lines in Fig. 6). Again, only the individual TO dampings were adjusted. Some difference between the two Ga-P dampings was permitted (less than 3 cm^{-1}), when needed to achieve optimum data modeling. A basic constraint that the Ga-As and Ga-P dampings should be similar (see Sec. IV B) is fulfilled at intermediate composition (e.g., at $x=0.56$ the dampings scale as 12:12), but relaxed in the dilute limits where the minor modes tend to become overdamped (e.g., at $x=0.85$ and 0.06, the dampings scale as 12:7 and 4:8, respectively). We stress that Fig. 2 holds for random As↔P substitution and that the fractions of individual oscillators therein are such that a basic conservation of the oscillator strength is fulfilled per bond and per alloy, by construction.

In summary, regarding the disconcerting IR reflectivity spectra of GaAsP, the percolation model explains as much as the cluster-VCA model, with (much) less adjustable parameters, and on the more realistic basis of a random As↔P substitution. With this, a long-standing paradox originating from the cluster approach that GaAsP seems highly segregated at the local scale with respect to its vibrational properties, and random otherwise, is naturally overcome.

V. CONCLUSION

We propose a simple version of the 1-bond→2-phonon percolation model for GaAsP with three oscillators, i.e., one MREI-like Ga-As mode at low frequency plus a distinct Ga-P doublet separated by ~12 cm^{-1}. This accounts for the puzzling multimode Raman and IR spectra of this alloy on a quantitative basis, while using no adjustable parameter basically, and by assuming random As↔P substitution. With this GaAsP and its like are rehabilitated as random alloys with respect to their vibrational properties, in principle. The study is supported by careful analysis of representative Raman and IR spectra in the literature, *ab initio* insight into the phonon modes of prototype impurity motifs, and existing EXAFS data.

This work brings to an end our systematic reexamination of the phonon behavior of the leading zincblende semiconductor alloys in the traditional VCA-based classification, which distinguishes between a "nominal" 1-bond→1-mode type for random alloys, divided in fact into three distinct subtypes [(i) pure 1-bond→1-mode, (ii) mixed-mode, (iii) modified 2-mode], as covered by the MREI model (macroscopic insight); plus an "anomalous" 1-bond→multimode type for nonrandom alloys as discussed within the (iv) 1-bond→4-mode cluster model (microscopic insight). We conclude to a universal 1-bond→2-mode behavior falling into the scope of a percolation paradigm (mesoscopic insight). Retrospectively, the original VCA paradigm seems either poor (MREI model) with respect to the natural complexity of the vibration spectra of alloys,[4] or just misleading (cluster model) regarding the nature of alloy disorder.

To complete an earlier figure that outlined the percolation schemes of the leading MREI alloys [subtypes (i) to (iii), see Fig. 5 of Ref. 4], we report in Fig. 7 the presently derived percolation scheme for GaAsP, the leading alloy of the remaining cluster-type (iv), as built up using the same format for sake of consistency. The Ga-As and Ga-P optical bands (shaded areas) are well separated, which is consistent with the Elliott-CPA (theoretical) classification of GaAsP as a type (i) system (see Sec. I).[2] Besides, the original cluster-type (experimental) classification of GaAsP as a multimode system, i.e., a three-mode one in fact if we refer to the IR reflectivity spectra of VB and CSP,[9,14] can be simply recovered as shown by ovals.

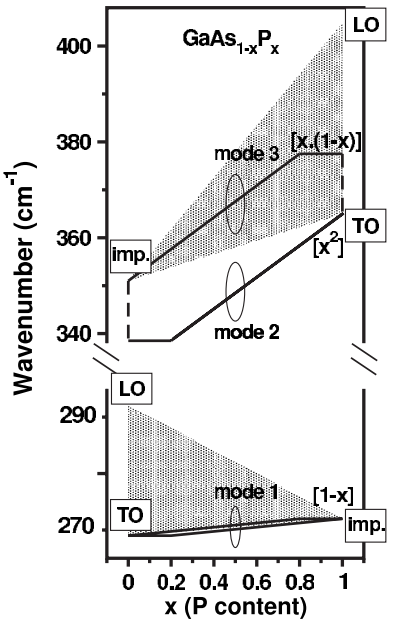

FIG. 7. Schematic view of the 1-bond→2-TO (thick lines) percolation scheme derived for GaAsP. The fractions of individual TO oscillators are indicated within brackets. The oblique rescaled-MREI segments are simplified to straight lines, for clarity. Shaded areas represent the TO-LO bands used for the Elliott's criterion. A direct comparison can be made with the percolation schemes of InGaAs, ZnTeSe, and InGaP, the systems representing the three admitted variants of the MREI type, as displayed in Fig. 5 of Ref. 4.

ACKNOWLEDGMENTS

The authors acknowledge support from the *Indo-French Centre for the Promotion of Advanced Research* (IFCPAR project No. 3204-1), and from the computing resources of the *Pôle Messin de Modélisation et de Simulation* (PMMS) of *Université Paul Verlaine—Metz*.

*Author to whom correspondence should be addressed; pages@univ-metz.fr

[1] D. W. Taylor, in *Optical Properties of Mixed Crystals*, edited by R. J. Elliott and I. P. Ipatova (North-Holland, Amsterdam, 1988), Chap. 2, p. 35.
[2] R. J. Elliott, J. A. Krumhansl, and P. L. Leath, Rev. Mod. Phys. **46**, 465 (1974).
[3] S. Baroni, S. De Gironcoli, and A. Dal Corso, Rev. Mod. Phys. **73**, 515 (2001).
[4] O. Pagès, A. V. Postnikov, M. Kassem, A. Chafi, A. Nassour, and S. Doyen, Phys. Rev. B **77**, 125208 (2008).
[5] R. Loudon, Adv. Phys. **13**, 423 (1964).
[6] J. C. Mikkelsen and J. B. Boyce, Phys. Rev. B **28**, 7130 (1983).
[7] M. Cardona, P. Etchegoin, H. D. Fuchs, and P. Molinà-Mata, J. Phys.: Condens. Matter **5**, A61 (1993).
[8] I. F. Chang and S. S. Mitra, Adv. Phys. **20**, 359 (1971).
[9] H. W. Verleur and A. S. Barker, Phys. Rev. **149**, 715 (1966).
[10] H. W. Verleur and A. S. Barker, Jr., Phys. Rev. **155**, 750 (1967).

[11] Not a pure VCA one though, strictly speaking, since the MREI description essentially supposes two distinct *A*-B and *A*-C TO branches, not a single (*A*-B, *A*-C)-mixed one attached to the parent modes. Note that the latter behavior may proceed from the MREI-VCA [referred to as type (ii) in the main text], it is just a matter to make the impurity modes coincide with the host TO modes in the MREI treatment.

[12] A. Mascarenhas, H. M. Cheong, M. J. Seong, and F. Alsina, in *Spontaneous Ordering in Semiconductor Alloys*, edited by A. Mascarenhas (Kluwer, New York, 2002), p. 391.

[13] B. Jusserand and S. Slempkes, Solid State Commun. **49**, 95 (1984).

[14] Y. S. Chen, W. Schockley, and G. L. Pearson, Phys. Rev. **151**, 648 (1966).

[15] The remaining five modes correspond to one acoustical mode (in-phase motion of *A*, B, and C atoms), which has no propagating character at $q \sim 0$, plus four optical modes due to out-of-phase vibrations of adjacent cluster units. Such modes vibrate at lower frequency than the bond-related ones, due to the large reduced mass of such cluster-type oscillator. Moreover, quoting VB, they are expected to have "*almost zero strength*" (Ref. 9, p. 722).

[16] Note that by extending the radius of the *A*-centered clusters beyond first neighbors each individual TO branch would further split so that in principle the cluster model leads to four TO modes per bond *at least*.

[17] A. Silverman, A. Zunger, R. Khalish, and J. Adler, Phys. Rev. B **51**, 10795 (1995).

[18] B. V. Robouch, A. Kisiel, and E. M. Sheregii, Phys. Rev. B **64**, 073204 (2001).

[19] A. Chafi, O. Pagès, A. V. Postnikov, J. Gleize, V. Sallet, E. Rzepka, L. H. Li, B. Jusserand, and J. C. Harmand, Appl. Phys. Lett. **91**, 051910 (2007).

[20] In fact the basic hypothesis of the cluster-VCA model that each VB cluster unit provides a unique vibration mode per bond is only valid in the limit case of the simplest cluster unit (containing a single impurity) immersed in the pure crystal of the other species. When departing from such highly dilute limit, where the symmetry is high, the picture collapses, and the impurity related phonon mode behavior becomes more complicated, even for that simplest cluster unit.

[21] A. V. Postnikov, O. Pagès, and J. Hugel, Phys. Rev. B **71**, 115206 (2005).

[22] O. Pagès, M. Ajjoun, T. Tite, D. Bormann, E. Tournié, and K. C. Rustagi, Phys. Rev. B **70**, 155319 (2004).

[23] D. Stauffer, *Introduction to Percolation Theory* (Taylor & Francis, London, 1985).

[24] N. D. Strahm and A. L. McWorter, in *Proceedings of the Conference on Light Scattering Spectra In Solids*, edited by G. B. Wright (Springer-Verlag, New York, 1969), p. 455.

[25] M. E. Pistol and X. Liu, Phys. Rev. B **45**, 4312 (1992).

[26] Z. Wu, K. Lu, Y. Wang, J. Dong, H. Li, C. Li, and Z. Fang, Phys. Rev. B **48**, 8694 (1993).

[27] R. Trommer, H. Müller, M. Cardona, and P. Vogl, Phys. Rev. B **21**, 4869 (1980).

[28] A. M. Teweldeberhan and S. Fahy, Phys. Rev. B **73**, 245215 (2006).

[29] A. Nassour, J. Hugel, and A. V. Postnikov, J. Phys.: Conf. Ser. **92**, 012139 (2007).

[30] J. M. Soler, E. Artacho, J. D. Gale, A. García, J. Junquera, P. Ordejón, and D. Sánchez-Portal, J. Phys.: Condens. Matter **14**, 2745 (2002) (http://www.uam.es/siesta).

[31] N. Troullier and J. L. Martins, Phys. Rev. B **43**, 1993 (1991).

[32] The maximum shift so far is ~ 40 cm^{-1}, as detected for the short and covalent Be-Se bond in ZnBeSe, that exhibits an unusually large contrast in bond properties. For a clear insight, compare Fig. 1 in Ref. 23 (experiment) with the inset of Fig. 6 in Ref. 4 (theory).

[33] L. Bellaiche, S. H. Wei, and A. Zunger, Phys. Rev. B **54**, 17568 (1996).

[34] G. D. Mahan, R. Gupta, Q. Xiong, C. K. Adu, and P. C. Eklund, Phys. Rev. B **68**, 073402 (2003).

[35] M. Cardona, in *Light Scattering in Solids II*, edited by M. Cardona and G. Güntherodt, Topics in Applied Physics Vol. 50 (Springer, Berlin, 1982), p. 62.

[36] D. J. Lockwood, G. Yu, and N. L. Rowell, Solid State Commun. **136**, 404 (2005).

[37] W. L. Faust and C. H. Henry, Phys. Rev. Lett. **17**, 1265 (1966).

[38] R. Cuscó, L. Artús, S. Hernández, J. Ibáñez, and M. Hopkinson, Phys. Rev. B **65**, 035210 (2001).

[39] H. Fu, V. Ozoliņš, and A. Zunger, Phys. Rev. B **59**, 2881 (1999).

[40] D. Schmeltzer and R. Beserman, Phys. Rev. B **22**, 6330 (1980).

[41] C. Hirlimann, R. Beserman and M. Balkanski, in *Proceedings of the Thirteenth International Conference on the Physics of Semiconductors*, edited by F. G. Fumi (Tipografia Marves, Rome, 1976), p. 208.

[42] K. P. Jain, R. K. Soni, and S. C. Abbi, Phys. Rev. B **31**, 6820 (1985).

[43] C. Ramkumar, K. P. Jain, and S. C. Abbi, Phys. Rev. B **54**, 7921 (1996).

[44] G. Armelles, M. J. Sanjuán, L. González, and Y. González, Appl. Phys. Lett. **68**, 1805 (1996).

[45] U. Fano, Rev. Mod. Phys. **64**, 313 (1992).